Complexion dictated thermal resistance with interface density in reactive metal multilayers

Christopher B. Saltonstall [1], Zachary D. McClure [2], Michael J. Abere,[1] David Guzman,[3] Samuel Temple Reeve,[4]
Alejandro Strachan,[2] Paul G. Kotula [1], David P. Adams,[1] and Thomas E. Beechem [1,5,*]

[1]*Sandia National Laboratories, Albuquerque, New Mexico 87185, USA*
[2]*School of Materials Engineering and Birck Nanotechnology Center, Purdue University, West Lafayette, Indiana 47907, USA*
[3]*Brookhaven National Laboratory, Condensed Matter Physics and Materials Science, Upton, New York, 11973, USA*
[4]*Materials Science Division, Lawrence Livermore National Laboratory, Livermore, California 94550, USA*
[5]*Center for Integrated Nanotechnologies, Sandia National Laboratories, Albuquerque, New Mexico 87185, USA*

Multilayers composed of aluminum (Al) and platinum (Pt) exhibit a nonmonotonic trend in thermal resistance with bilayer thickness as measured by time domain thermoreflectance. The thermal resistance initially increases with reduced bilayer thickness only to reach a maximum and then decrease with further shrinking of the multilayer period. These observations are attributed to the evolving impact of an intermixed amorphous complexion approximately 10 nm in thickness, which forms at each boundary between Al- and Pt-rich layers. Scanning transmission electron microscopy combined with energy dispersive x-ray spectroscopy find that the elemental composition of the complexion varies based on bilayer periodicity as does the fraction of the multilayer composed of this interlayer. These variations in complexion mitigate boundary scattering within the multilayers as shown by electronic transport calculations employing density-functional theory and nonequilibrium Green's functions on amorphous structures obtained via finite temperature molecular dynamics. The lessening of boundary scattering reduces the total resistance to thermal transport leading to the observed nonmonotonic trend thereby highlighting the central role of complexion on thermal transport within reactive metal multilayers.

I. INTRODUCTION

Multilayers are ubiquitous across the materials landscape being used to tune all manners of properties. Functionally, the properties of multilayers emerge from the spacing and materials composing the many interfaces implicit in layered solids. These boundaries can affect the wave nature of the energy carriers themselves while also impacting their scattering. Changes in the energy carriers (e.g., photons, phonons, electrons)—and their scattering—necessarily dictate properties. For example, in optical coatings, the spacing and refractive indices of material layers are chosen to create constructive or destructive interference of photons over a selected wavelength range. A similar goal is aspired to when using multilayers in thermoelectrics. In this case, the objective is to minimize phonon transport through scattering across the entire phonon spectrum. To this end, multilayers exhibiting extremely low thermal conductivity have been achieved by leveraging Van der Waals bonds [1], nanolamination [2], and nanostructuring [3].

Regardless of approach, the reported reductions in thermal conductivity evolve from scattering at interfaces consistent with the view that heat transport obeys a series resistor model where the total thermal resistance is proportional to the number of material boundaries. This view is not strictly valid, however. The paradigm presumes that every interface

between two materials offers the same amount of thermal resistance. Reality is not so simple. Variations in disorder [4–7], composition [8,9], and changes in bonding [10,11] between interfaces can all affect transport. Each of these characteristics, in turn, is subject to processing, environment, and even the spacing between boundaries. Taken together, thermal transport through a multilayer will therefore be intimately tied to interfacial structure and its evolution.

Despite numerous studies for phonon dominated systems where interfacial disorder has been shown to both [12] increase [6,13] and decrease [4,5,14] boundary conductance, the impact of interfacial structure on thermal transport in electron dominated systems has not been addressed in nearly as much detail. Within several metal multilayers, a thin ($\sim$10 nm) compositionally mixed volume exists at each boundary [15]. This intermixed interlayer—termed a complexion [16]—profoundly impacts a wide breadth of properties ranging from grain growth and fracture strength to ionic conductivity and electron mobility [17]. The impact of complexion on thermal transport, especially within electron-dominated systems, remains largely unexplored, however. To address this gap, we investigate here the influence of periodicity and interfacial structure on the thermal resistance of metal multilayers to highlight the predominant role of complexion, and more generally disorder, on heat transport within electron-dominated multilayers.

Practically, the thermal conductivity of Al/Pt metal multilayers with varying bilayer period thickness was measured using time-domain thermoreflectance (TDTR) and simulated

_____
*tebeech@sandia.gov

under a nonequilibrium Green's functions (NEGF) framework in which the multilayers are described through a combination of molecular dynamics (MD) and density-functional theory (DFT). Due to the preference of Al and Pt to be fully alloyed, a 10-nm region of amorphous intermixing (i.e., a complexion) exists at each material transition. This intermixing has a significant effect on the thermal transport, most notably inducing a nonmonotonic trend in thermal resistance with the bilayer period thickness. While this observation cannot be explained using traditional approaches such as the electron diffuse mismatch model (eDMM), it evolves due to the changing complexion of the multilayer as its periodicity is altered.

II. MATERIAL AND METHODS

A. Multilayer synthesis

Multilayers were grown by sputtering Al and Pt with a period thicknesses ranging from 6 to 800 nm [128 to 1 bilayer period(s)] atop a silicon substrate. All films had a total thickness of ≈ 800 nm. Details of the growth and structural characterization via x-ray diffraction (XRD) and transmission electron microscopy are described in the Supplemental Material [18]. Specifically, the Supplemental Material provides details regarding growth and characterization of multilayer films [19–21], thermal measurements [22], and first-principles-based modeling [23–26]. Due to the lower potential energy of the fully mixed phase compared to the segregated multilayer, the Al and Pt layers spontaneously intermix to form a compositionally graded region approximately 10 nm thick at each boundary between them. This intermixed region is a complexion, which describes a finite layer forming at the boundary between two bulk phases [15]. To further specify, the Al/Pt system forms a nanolayer complexion under the Dillon-Harmer taxonomy due to its near constant 10-nm thickness irrespective of the bilayer period [27]. The complexion thickness is comparable to other bimetallic systems [15]. Hereafter, the terms complexion and interlayer will be used synonymously. Regardless of nomenclature, this interlayer, or complexion, is amorphous as is observed through electron diffraction and emerges when the minority elemental species exceeds $\approx 10\%$ as shown in the Supplemental Material [28]. Having a constant interlayer thickness, multilayers with periods below 20 nm are therefore effectively composed of only the complexion.

Energy dispersive x-ray spectroscopy (EDS) composition traces, meanwhile, indicate that not only is the crystallinity of the multilayer impacted by the periodicity but so too the composition of the films. With decreasing bilayer thickness, the composition no longer possesses regions of the pure metal layers but is instead an alloy of Al_xPt_{1-x} that varies in its composition as is seen in Fig. 2. Due to this observation, monolithic Al_xPt_{1-x} alloys were also synthesized via sputtering codeposition to thicknesses of ≈ 800 nm. These monolithic films were pursued to both validate the computational approaches described in the proceeding sections and assess the intrinsic thermal resistance of the interlayer apart from the boundaries. All films, both those monolithic and multilayer, were capped with a ≈ 80-nm Al layer—denoted subsequently as the cap—to facilitate thermal characterization as is shown in Fig. 1.
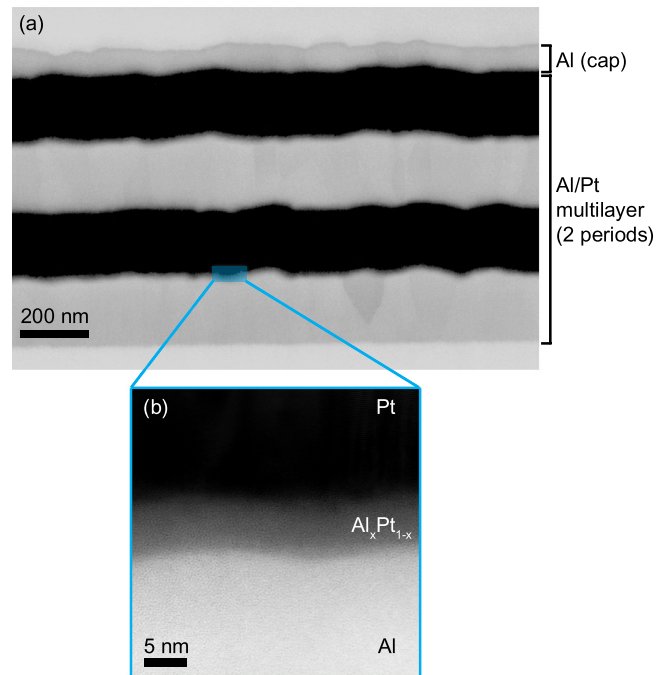
FIG. 1. (a) Bright-field scanning transmission electron microscopy images of cross-sectioned Al/Pt metal multilayer obtained at (a) a low magnification sufficient to view through the entire thickness and (b) high magnification that distinguishes a ≈ 10-nm-thick complexion that exists at each boundary. This interlayer region is amorphous as indicated by electron diffraction (see Supplemental Material Fig. S2). The rectangle in (a) represents a nominal location for (b) and is not exact.

B. Thermal measurements

Thermal resistance measurements were performed using TDTR. A detailed description of the experimental setup can be found elsewhere [29,30] and in the Supplemental Material. The ratio of the in-phase to out-of-phase response was fit to a three-layer model where the multilayer was assumed to be an effective medium [31]. The Al-cap/multilayer boundary conductance and thermal conductivity of the effective medium representing the multilayer were left as free parameters and fit to the acquired data. The total resistance of the multilayer film was then taken to be the sum of the Al to multilayer boundary resistance and that of the effective medium. Results are tabulated in Table I, where it is seen that thermal resistance does not monotonically increase with the number of periods. The causes for this nonmonotonic trend will be discussed in detail via modeling of the system as is described subsequently.

C. Modeling and simulation

To provide insight into the physical mechanisms behind the experimental observations, multilayer thermal resistance was predicted under two different computational paradigms. First, the traditional eDMM was employed within a series resistance paradigm, where boundaries are presumed abrupt and interfaces perfect with energy transmission determined based on density of states overlap between the two materials making up the boundary [14]. As will be described below, this simple model fails to capture the experimental observations,

TABLE I. Characteristics of examined Al/Pt multilayers accompanied by measured and NEGF+DFT predicted thermal resistances.

Number of periods	Period thickness (ca.) (nm)	Exp. resistance (m²K/MW)	NEGF resistance (m²K/MW)
1	800	0.024	
2	400	0.024	
4	200	0.038	0.019
8	100	0.050	0.030
16	50	0.11	0.06
32	25	0.15	0.11
48	16.7	0.16	
64	12.5	0.12	0.10
96	8.3	0.14	0.103
128	6.25	0.10	0.102

even for long-period superlattices. This is not surprising given the complexity of the structures involved. To account for this complexity, a first-principles-based multiscale approach was developed to describe thermal transport that was capable of explicitly describing the complexion and the contact resistance between the regions. Molecular dynamics simulations were employed to predict atomistic structures of the Al_xPt_{1-x} alloys observed in the complexion and capture the effect of thermal ionic fluctuations on transport [32]. Thermal transport in these structures was then modeled using NEGF within the Landauer approximation leveraging electronic structure obtained from DFT calculations [33].

In both the eDMM and first-principles calculations, the complexion resistance was quantified and then the total thermal resistance of the multilayer film (R_{Tot}) determined using a series resistance model given by [34]

$$R_{Tot} = R_0 + nR_{BD}, \qquad (1)$$

where R_0 is the resistance of the constituent material layers ($R_o = R_{Pt} + R_{Al}$) and n is the number of material transitions given by $n = 2P + 1$ where P is the number of periods. R_{BD} is the total thermal resistance of the complexion. Practically, the resistance of Al and Pt was determined using separate NEGF + DFT simulations of pure crystalline layers using methods previously employed [35]. The methodology to determine the complexion resistance, meanwhile, differed based on the technique employed as is described below.

1. eDMM

The eDMM is based on free electron theory and can be written as [14]:

$$\frac{1}{R_{BD,eDMM}} = \frac{1}{4}\zeta_{Al \to Pt} C_{e,Al} v_{F,Al}, \qquad (2)$$

where C_e is the electronic heat capacity and v_F is the Fermi velocity. The specific heat is given by:

$$C_e = \frac{\pi^2}{3}D(\epsilon_F)k_B^2 T, \qquad (3)$$

where k_B is Boltzmann's constant, T is temperature, and $D(\epsilon_F)$ is the density of states at the Fermi energy. The
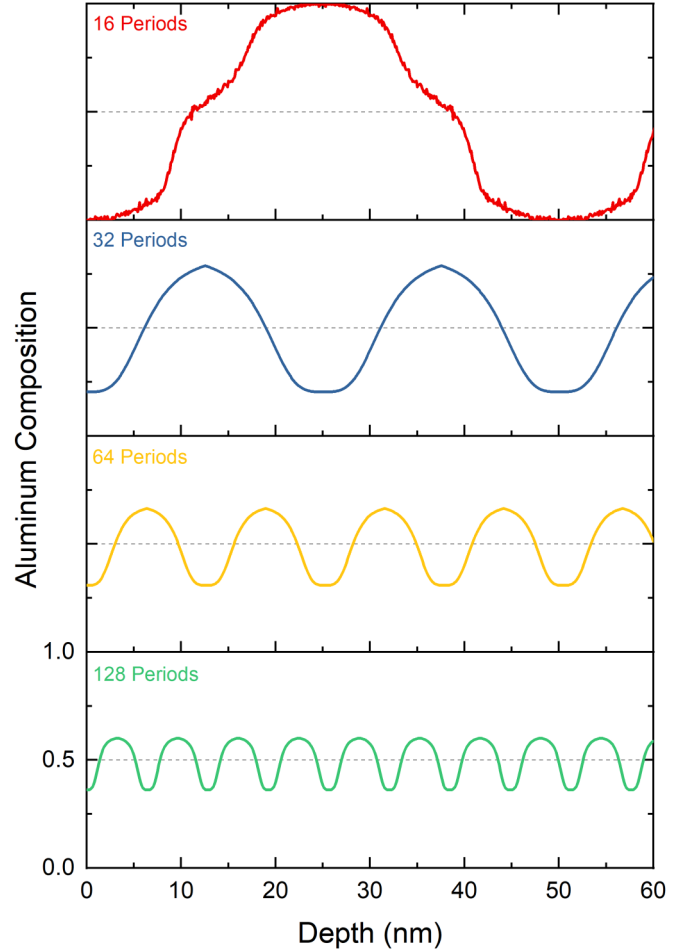
FIG. 2. EDS-derived compositional maps of Al/Pt multilayers possessing varying number of periods. The composition range decreases as the period thickness decreases.

transmission coefficient is

$$\zeta_{Al \to Pt} = \frac{D(\epsilon_{F,Pt})v_{F,Pt}}{D(\epsilon_{F,Pt})v_{F,Pt} + D(\epsilon_{F,Al})v_{F,Al}}, \qquad (4)$$

where $Al \to Pt$ denotes transport from Al to Pt. Since the interface is, in reality, an alloyed metal complexion, thermal transport was assumed to be dominated by electron transport as is implied by this approach. The resulting Kapitza resistance derived by the eDMM was calculated to be $R_{BD,eDMM} = 0.18$ m²K/GW. The material parameters used for this calculation are presented in the Supplemental Material.

2. First-principles-based atomistic simulations

The eDMM assumes pristine, atomically sharp, interfaces. However, there is significant intermixing in the multilayers considered here as a finite complexion forms. As shown in Fig. 1 and 2, this region has both finite thickness and variable composition. Therefore, a more detailed description of the electronic transport through the complexion and the associated contacts must be considered. Given the smooth variation in composition observed experimentally, our approach involves computing the thermal resistivities of Al_xPt_{1-x} alloys of various compositions from first principles
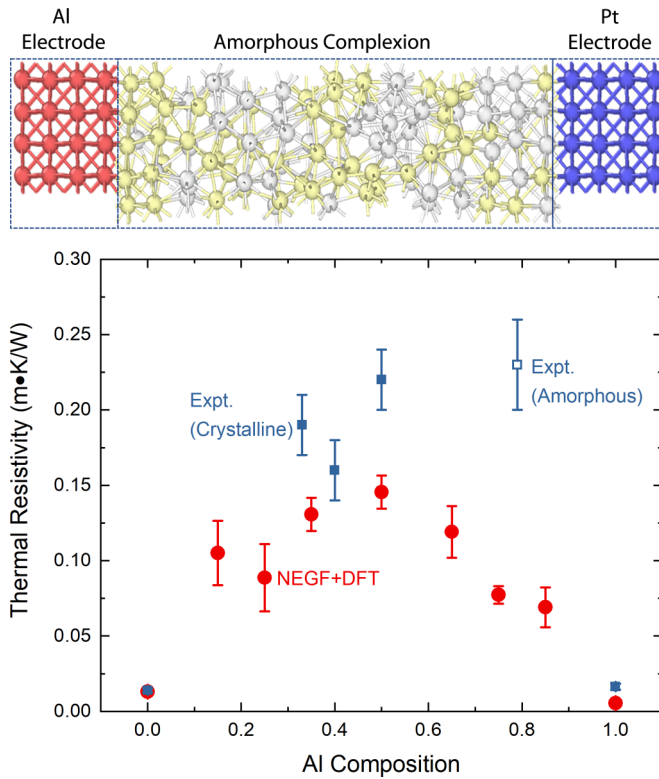
FIG. 3. Top: Representative atomic structure of simulation domain realized through molecular dynamics. Bottom: Comparison of computationally derived thermal resistance of amorphous Al_xPt_{1-x} alloys compared to experimental results of monolithic films measured using TDTR.

and combining them in series to predict thermal transport of the complexion as a whole. Importantly, the simulations also quantify the contact resistance involved in transitioning between the crystalline Al or Pt and the amorphous interlayer region (i.e., Kapitza resistance).

To capture the compositional and structural variability of the complexion, MD simulations were employed to melt and quench an Al/Pt alloy of a given composition to obtain relaxed, but heavily disordered, structures like those observed experimentally. The resulting disordered alloy is situated between crystalline Al and Pt contacts as shown in Fig. 3. Subsequently, the MD-derived atomic arrangements were utilized within the NEGF/Landauer transport formalism using electronic structures obtained from DFT calculations. Thermal resistance of the Al/complexion/Pt system was then obtained from these NEGF transport simulations. Details surrounding each of these computational steps—MD-derived structural generation, DFT deduced electronic structure, and NEGF transport calculations—are provided subsequently.

The compositional domain was made up of Al and Pt leads separated by a Al_xPt_{1-x} channel representing a given composition across the range observed in Fig. 2. The leads consist of perfect face-centered cubic crystals oriented along [100], replicated in a $2 \times 2 \times 2$ arrangement, and having an averaged lattice parameter between that of Al and Pt (3.98 Å). The averaged lattice parameter was used to ensure minimal strain on the contacts between the leads and channel. The

leads are separated by a channel having the desired alloy composition. In practice, seven different Al_xPt_{1-x} alloy compositions were characterized using channel lengths varying from 1.4 to 3.0 nm. The amorphous layer was generated by melting the channel at $T = 3000$ K via isochoric isothermal MD simulations and then quenched to room temperature in 10 ps while keeping the leads fixed. Subsequently, MD simulations of this quenched structure were performed at 300 K to capture elastic phonon-electron coupling (i.e., thermal ionic fluctuations) [32]. All MD simulations were carried out with LAMMPS [36,37] using an effective medium theory potential developed by Jacobsen *et al.* [38].

The electronic structure required for the NEGF calculations was obtained using the MD-derived atomic arrangement via DFT carried out using the TranSIESTA code [33] implemented in the SIESTA package [39,40]. With this approach, core electrons are replaced by pseudopotentials, and the valence electrons are represented using a numerical, atomic-like, basis set. The exchange-correlation potential is calculated within the generalized gradient approximation functional [41]. Double zeta plus polarization numerical orbital basis sets were used for all atomic species.

The resulting DFT-derived electronic structure was employed to deduce transport properties by utilizing NEGF within the Landauer approximation. Functionally, NEGF simulates electrons' movement from a crystalline aluminum contact through the interlayer and to a crystalline Pt contact. By simulating a series of films possessing identical compositions but of varying length, the thermal resistance was quantified through the slope of resistance versus film thickness [32]. The intercept of this linear fit, meanwhile, provides an estimate of the combined Al/complexion and complexion/Pt Kapitza resistance, which is also dependent on composition. Full details for all steps of the simulation are described in the Supplemental Material.

Figure 3 shows the calculated resistivities of Al_xPt_{1-x} alloys having variable composition. End points correspond to transport through fully crystalline Al and Pt channels. These "pure" systems were used as validation and calculated to be 185 and 76 W m^{-1} K^{-1} for Al and Pt, respectively. The values compare favorably to accepted values [42] and those measured for "pure" Al or Pt films deposited in an analogous manner to that of the multilayers. Thermal resistance of Al_xPt_{1-x} alloys calculated via the NEGF + DFT approach compares well to experimental measurements of monolithic films as seen in Fig. 3 lending further credence to the methodology employed. The correlation to within a factor of three is notable considering the differences in that simulated versus that measured. The model, for instance, does not account for nanovoiding existing within the actual films. The codeposited films, meanwhile, begin to crystallize at higher Pt compositions as was confirmed using XRD whereas the simulation cell maintains an overwhelmingly amorphous structure similar to that observed within the complexion of the multilayers. Taken together, the computational approach therefore provides a reasonable description of transport through the complexion. Specifically, it accounts for its compositional dependence as is seen by the "inverted-bathtub" shape of Fig. 3.

These compositionally dependent thermal resistances were then used to calculate the total complexion resistance

($R_{\text{BD,NEGF+DFT}}$) in a manner that included both the variation in composition and the finite width of the complexion. This was realized by first discretizing the compositional maps shown in Fig. 2 in 0.1-nm steps. Using the average composition within a given step, the resistance was calculated for this discretized region using values supplied from the simulations of Fig. 3. The total complexion resistance was then realized via a series sum of the discrete elements while also including the Kapitza resistance existing between the metallic end members and the complexion. Mathematically, this is described as shown in Eq. (5),

$$R_{\text{BD,NEGF+DFT}} = \sum_{i}^{n} \frac{d_i}{\kappa(x_i)} + R_{\text{Kapitza}}, \qquad (5)$$

where d and $\kappa(x_i)$ are the thickness- and composition-dependent thermal conductivity of the ith element, respectively, and R_{Kapitza} is the total Kapitza resistance accounting for boundaries between the complexion and both Al and Pt. Quantitatively, a compositional average of 0.28 m^{2}K/GW derived from the NEGF + DFT was employed for R_{Kapitza}. The Kapitza resistance was considered only for films where regions of pristine Al and Pt exist on either side of the complexion and was thus excluded when the period thickness was sufficiently small (< 20 nm) that the film was composed entirely of the compositionally varying interlayer.

The choice to simulate individual compositions and leverage the series model of Eq. (5) is advantageous for several reasons. First, it eliminates the need to generate realistic atomistic structures under rigid constraints describing the observed complexion thickness and compositional gradient. Second, discretization dramatically reduces the compositional cost by capturing the bulk behavior apart from having to simulate the entirety of the 800-nm multilayer. While domains of this size can be simulated using traditional NEGF calculations, the *ab initio* approach employed here makes simulating the entire multilayer far less practical. It is noteworthy that the 0.1-nm steps used to discretize the complexion are far less than the electron mean free path. The composition specific thermal resistances applied to each discretized region were, however, obtained from simulations of variable domain length to ensure a "bulk" response. The discretized approach therefore provides a means to accurately account for the compositional gradient in a computationally efficient manner apart from artificially imparting size effects into the simulation.

III. RESULTS

Figure 4 plots the experimental and computationally derived total thermal resistance of the multilayers as a function of the number of bilayer periods. Experimentally, the resistance initially increases linearly with the number of periods where it rolls over after reaching a maximum resistance at about 48 periods, corresponding to a bilayer thickness of 17 nm (i.e., $\sim 2\times$ the complexion thickness). Subsequently, the resistance decreases to a value that is on par with the simulated Al$_{50}$Pt$_{50}$ alloyed film whose resistance was shown in Fig. 3. While the rollover in thermal resistance is qualitatively similar to that seen previously in phonon dominated systems [43], its causation is of wholly different character. Here the rollover
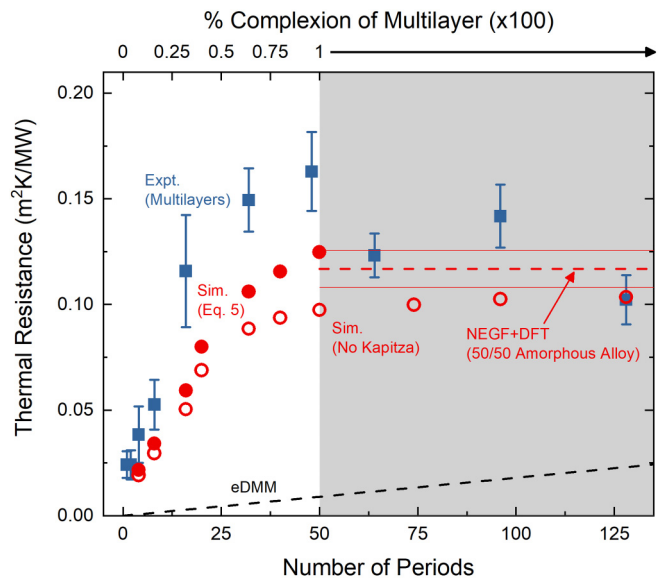
FIG. 4. Thermal resistance of Al/Pt metal multilayers as measured by TDTR and simulated using both eDMM and NEGF + DFT approaches. Measured resistance reaches a peak with 48 periods and then decreases. Unlike the eDMM which assumes a perfect interface, the NEGF + DFT approach captures this behavior by accounting for both the finite width and variable composition of the complexion. With increasing number of periods, the multilayer film approaches exhibits a thermal resistance on par with that modeled for an amorphous alloy of approximately 50/50 composition.

in thermal resistance originates due to alterations in the complexion that emerge with changes in the multilayer period. The following provides evidence supporting this assertion.

Predictions of thermal interface resistance of electron dominated systems have overwhelmingly used the eDMM, which presumes a perfect interface resulting in a monotonically increasing trend in total resistance stemming from Eq. (1). As seen from Fig. 4, this approach is contrary to observation both qualitatively and quantitatively despite estimating a Kapitza resistance that is within a factor of 2 of that derived using the NEGF + DFT approach. The NEGF + DFT approach, in contrast to the eDMM, does predict the observed nonlinear trend in thermal resistance while also comparing quite well to experiment. Since the Kapitza resistances are quite similar between the techniques, the discrepancy points to the the centrality of the complexion on thermal transport for which only the NEGF + DFT approach "sees."

Examining alterations in the complexion with bilayer period therefore provides a means to understand the causation of the nonmonotonic thermal resistance trend. Structurally, the relative amount of complexion making up the multilayer is dependent on period due to the rather constant (~ 10 nm) thickness of the interlayer. This is in contrast to the extent of the Al and Pt layers themselves, which continually decrease in thickness with increasing period number. Quantitatively, the finite thickness of the complexion means that the volume percentage of the complexion within the multilayer increases with the number of periods as is highlighted in the upper axis of Fig. 4. In addition, changes in the multilayer periodicity

alter the composition of the complexion as is apparent by examining Fig. 2.

These period-dependent changes of composition and structure within the complexion each impact thermal transport. For example, the complexion has a thermal resistance that is heavily dependent on composition as exhibited in Fig. 3. Changes in composition of the complexion as seen in Fig. 2 will thus necessarily impact the total thermal resistance of the multilayer. Increasing the relative amount of the interlayer, meanwhile, impacts thermal transport for two reasons. First, the complexion necessarily has a higher thermal resistance than does the pure crystalline metallic components. Second, increasing amounts of the complexion act to "soften" the material contrast at the boundaries and then remove the boundaries altogether as the "multilayer" becomes effectively a film composed entirely of the complexion. In the language of thermal transport, the increasing amount of complexion in the multilayer acts to reduce and then eventually remove the Kapitza resistance [6].

To highlight this fact, NEGF + DFT-derived thermal resistances were calculated apart from the contribution of the Kapitza resistance stemming from the boundaries between amorphous alloy and the crystalline Al and Pt [i.e., $R_{\mathrm{BD,NEGF+DFT}}$ in Eq. (5)]. These resistances are represented by the open circles of Fig. 4 where the values smoothly approach the resistance of the modeled monolithic 50/50 alloy. The simulations accounting for the Kapitza resistance (closed circles of Fig. 4), meanwhile, exhibit a steeper trend with the number of periods while also correlating well to the measured results for the region where boundaries persist between the pure metals and the interlayer. The differences between the two curves, in turn, are indicative of the reduced role that boundary scattering plays with increasing period number. We therefore stipulate that the observed rollover in thermal resistance occurs because scattering transforms from being mediated through boundary scattering at larger bilayer thickness to one in which point-defect scattering implicit to the complexion dictates transport. The disorder mediated by the complexion has acted to not just change the structure of the film but so too the dominant transport mechanism.

At a higher level, this observation emphasizes not only the central role that complexion may have on electron-dominated thermal systems but also underscores the sometimes counterintuitive role that boundaries play on thermal transport. More is not necessarily bigger. Increasing the number of boundaries is not inextricably linked to reduced thermal transport even in electron dominated systems. Rather, as the number of boundaries increase, the physical processes belying the movement of energy can change as well. This change can actually increase the efficiency by which heat is moved. Here, disorder stemming from finitely sized complexions existing between Al and Pt layers acted to enhance heat transport even as the number of material boundaries increased.

IV. CONCLUSIONS

A complexion—i.e., an amorphous interlayer—existing between adjacent regions of a material dictates thermal transport in Al/Pt multilayers. This was deduced by observing a nonmonotonic trend in thermal resistance as the number of periods increased in these multilayers. To understand this reduction in thermal resistance with increasing period number, structural characterization of the films was combined with simulations leveraging density-functional theory in concert with nonequilibrium Green's functions to describe the transport. Taken together, these efforts show that intermixing occurs at the Al/Pt boundary leading to the creation of a $\sim$10 nm amorphous nanolayer complexion at every boundary. The complexion dominates transport within the multilayers facilitating a transformation from boundary- to point-defect scattering that acts to ultimately reduce thermal resistance. Engineering complexion is therefore a viable route to controlling thermal transport even in electron-dominated systems.

[1] C. Chiritescu, D. G. Cahill, N. Nguyen, D. Johnson, A. Bodapati, P. Keblinski, and P. Zschack, Ultralow thermal conductivity in disordered, layered WSe$_2$ crystals, Science **315**, 351 (2007).

[2] R. Costescu, D. G. Cahill, F. Fabreguette, Z. Sechrist, and S. George, Ultra-low thermal conductivity in W/Al$_2$O$_3$ nanolaminates, Science **303**, 989 (2004).

[3] B. Poudel, Q. Hao, Y. Ma, Y. Lan, A. Minnich, B. Yu, X. Yan, D. Wang, A. Muto, D. Vashaee, X. Chen, J. Liu, M. S. Dresselhaus, G. Chen, and Z. Ren, High-thermoelectric performance of nanostructured bismuth antimony telluride bulk alloys, Science **320**, 634 (2008).

[4] T. Beechem, S. Graham, P. Hopkins, and P. Norris, Role of interface disorder on thermal boundary conductance using a virtual crystal approach, Appl. Phys. Lett. **90**, 054104 (2007).

[5] P. E. Hopkins, P. M. Norris, R. J. Stevens, T. E. Beechem, and S. Graham, Influence of interfacial mixing on thermal boundary conductance across a chromium/silicon interface, J. Heat Transfer **130**, 062402 (2008).

[6] T. Beechem and P. E. Hopkins, Predictions of thermal boundary conductance for systems of disordered solids and interfaces, J. Appl. Phys. **106**, 124301 (2009).

[7] P. E. Hopkins, L. M. Phinney, J. R. Serrano, and T. E. Beechem, Effects of surface roughness and oxide layer on the thermal boundary conductance at aluminum/silicon interfaces, Phys. Rev. B **82**, 085307 (2010).

[8] J. C. Duda, T. S. English, E. S. Piekos, T. E. Beechem, T. W. Kenny, and P. E. Hopkins, Bidirectionally tuning kapitza conductance through the inclusion of substitutional impurities, J. Appl. Phys. **112**, 073519 (2012).

[9] C. S. Gorham, K. Hattar, R. Cheaito, J. C. Duda, J. T. Gaskins, T. E. Beechem, J. F. Ihlefeld, L. B. Biedermann, E. S. Piekos, D. L. Medlin, and P. E. Hopkins, Ion irradiation of the native oxide/silicon surface increases the thermal boundary conductance across aluminum/silicon interfaces, Phys. Rev. B **90**, 024301 (2014).

[10] M. D. Losego, M. E. Grady, N. R. Sottos, D. G. Cahill, and P. V. Braun, Effects of chemical bonding on heat transport across interfaces, Nat Mater **11**, 502 (2012).

[11] P. E. Hopkins, M. Baraket, E. V. Barnat, T. E. Beechem, S. P. Kearney, J. C. Duda, J. T. Robinson, and S. G. Walton, Manipulating thermal conductance at metal-graphene contacts via chemical functionalization, Nano Lett. **12**, 590 (2012).

[12] P. E. Hopkins, Thermal transport across solid interfaces with nanoscale imperfections: Effects of roughness, disorder, dislocations, and bonding on thermal boundary conductance, ISRN Mech. Eng. **2013**, 682586 (2013).

[13] R. J. Stevens, L. V. Zhigilei, and P. M. Norris, Effects of temperature and disorder on thermal boundary conductance at solid-solid interfaces: Nonequilibrium molecular dynamics simulations, Int. J. Heat Mass Transf. **50**, 3977 (2007).

[14] B. C. Gundrum, D. G. Cahill, and R. S. Averback, Thermal conductance of metal-metal interfaces, Phys. Rev. B **72**, 245426 (2005).

[15] J. D. Schuler and T. J. Rupert, Materials selection rules for amorphous complexion formation in binary metallic alloys, Acta Mater. **140**, 196 (2017).

[16] S. J. Dillon, M. Tang, W. C. Carter, and M. P. Harmer, Complexion: a new concept for kinetic engineering in materials science, Acta Mater. **55**, 6208 (2007).

[17] A. R. Krause, P. R. Cantwell, C. J. Marvel, C. Compson, J. M. Rickman, and M. P. Harmer, Review of grain boundary complexion engineering: Know your boundaries, J. Am. Ceram. Soc. **102**, 778 (2019).

[18] See Supplemental Material at http://link.aps.org/supplemental/10.1103/PhysRevB.101.245422 for details regarding: growth and characterization of multilayer films [19–21], thermal measurements [22], and first-principles-based modeling [23–26].

[19] D. Adams, R. Reeves, M. Abere, C. Sobczak, C. Yarrington, M. Rodriguez, and P. Kotula, Ignition and self-propagating reactions in Al/Pt multilayers of varied design, J. Appl. Phys. **124**, 095105 (2018).

[20] D. Adams, M. Rodriguez, C. Tigges, and P. Kotula, Self-propagating, high-temperature combustion synthesis of rhombohedral alpt thin films, J. Mater. Res. **21**, 3168 (2006).

[21] B. Blanpain, L. H. Allen, J. M. Legresy, and J. W. Mayer, Solid-state amorphization in Al-Pt multilayers by low-temperature annealing, Phys. Rev. B **39**, 13067 (1989).

[22] Z. Lin, L. V. Zhigilei, and V. Celli, Electron-phonon coupling and electron heat capacity of metals under conditions of strong electron-phonon nonequilibrium, Phys. Rev. B **77**, 075133 (2008).

[23] P. M. Larsen, S. Schmidt, and J. Schiøtz, Robust structural identification via polyhedral template matching, Modell. Simul. Mater. Sci. Eng. **24**, 055007 (2016).

[24] A. Stukowski, Visualization and analysis of atomistic simulation data with ovito-the open visualization tool, Modell. Simul. Mater. Sci. Eng. **18**, 015012 (2009).

[25] O. K. Andersen, Electronic structure of the fcc transition metals Ir, Rh, Pt, and Pd, Phys. Rev. B **2**, 883 (1970).

[26] N. Troullier and J. Martins, A straightforward method for generating soft transferable pseudopotentials, Solid State Commun. **74**, 613 (1990).

[27] P. R. Cantwell, M. Tang, S. J. Dillon, J. Luo, G. S. Rohrer, and M. P. Harmer, Grain boundary complexions, Acta Mater. **62**, 1 (2014).

[28] D. Adams, Reactive multilayers fabricated by vapor deposition: A critical review, Thin Solid Films **576**, 98 (2015).

[29] T. E. Beechem, A. E. McDonald, E. J. Fuller, A. Alec Talin, C. M. Rost, J.-P. Maria, J. T. Gaskins, P. E. Hopkins, and A. A. Allerman, Size dictated thermal conductivity of gan, J. Appl. Phys. **120**, 095104 (2016).

[30] C. D. Landon, R. H. T. Wilke, M. T. Brumbach, G. L. Brennecka, M. Blea-Kirby, J. F. Ihlefeld, M. J. Marinella, and T. E. Beechem, Thermal transport in tantalum oxide films for memristive applications, Appl. Phys. Lett. **107**, 023108 (2015).

[31] R. Cheaito, K. Hattar, J. T. Gaskins, A. K. Yadav, J. C. Duda, T. E. Beechem, J. F. Ihlefeld, E. S. Piekos, J. K. Baldwin, and A. Misra, Thermal flux limited electron kapitza conductance in copper-niobium multilayers, Appl. Phys. Lett. **106**, 093114 (2015).

[32] T. Markussen, M. Palsgaard, D. Stradi, T. Gunst, M. Brandbyge, and K. Stokbro, Electron-phonon scattering from green's function transport combined with molecular dynamics: Applications to mobility predictions, Phys. Rev. B **95**, 245210 (2017).

[33] M. Brandbyge, J.-L. Mozos, P. Ordejón, J. Taylor, and K. Stokbro, Density-functional method for nonequilibrium electron transport, Phys. Rev. B **65**, 165401 (2002).

[34] B. C. Daly, H. J. Maris, K. Imamura, and S. Tamura, Molecular dynamics calculation of the thermal conductivity of superlattices, Phys. Rev. B **66**, 024301 (2002).

[35] D. M. Guzman and A. Strachan, Enhanced electron transport in thin copper films via atomic-layer materials capping, arXiv:1805.01517 (2018).

[36] S. Plimpton, Fast parallel algorithms for short-range molecular dynamics, J. Comput. Phys. **117**, 1 (1995).

[37] L.-S. Atomic and M. M. P. Simulator, LAMMPS, http:/lammps.sandia.gov, 2013.

[38] K. W. Jacobsen, P. Stoltze, and J. Nørskov, A semi-empirical effective medium theory for metals and alloys, Surf. Sci. **366**, 394 (1996).

[39] P. Ordejón, E. Artacho, and J. M. Soler, Self-consistent order-n density-functional calculations for very large systems, Phys. Rev. B **53**, R10441 (1996).

[40] J. M. Soler, E. Artacho, J. D. Gale, A. García, J. Junquera, P. Ordejón, and D. Sánchez-Portal, The siesta method forab initioorder-nmaterials simulation, J. Phys.: Condens. Matter **14**, 2745 (2002).

[41] J. P. Perdew, K. Burke, and M. Ernzerhof, Generalized Gradient Approximation Made Simple, Phys. Rev. Lett. **77**, 3865 (1996).

[42] R. Powell, C. Y. Ho, and P. E. Liley, *Thermal Conductivity of Selected Materials*, Vol. 8 (US Department of Commerce, National Bureau of Standards Washington, DC, 1966).

[43] J. Ravichandran, A. K. Yadav, R. Cheaito, P. B. Rossen, A. Soukiassian, S. Suresha, J. C. Duda, B. M. Foley, C.-H. Lee, and Y. Zhu, Crossover from incoherent to coherent phonon scattering in epitaxial oxide superlattices, Nat. Mater. **13**, 168 (2014).